SIAM J. SCI. COMPUT.
Vol. 19, No. 2, pp. 404–425, March 1998

005

ENHANCED CELL-CENTERED FINITE DIFFERENCES FOR ELLIPTIC EQUATIONS ON GENERAL GEOMETRY*

TODD ARBOGAST[†,‡], CLINT N. DAWSON[†,§], PHILIP T. KEENAN[†], MARY F. WHEELER[†,§,¶], AND IVAN YOTOV[†,♣]

Abstract. We present an expanded mixed finite element method for solving second order elliptic partial differential equations on geometrically general domains. For the lowest-order Raviart-Thomas approximating spaces, we use quadrature rules to reduce the method to cell-centered finite differences, possibly enhanced with some face-centered pressures. This substantially reduces the computational complexity of the problem to a symmetric, positive definite system for essentially only as many unknowns as elements. Our new method handles general shape elements (triangles, quadrilaterals, and hexahedra) and full tensor coefficients, while the standard mixed formulation reduces to finite differences only in special cases with rectangular elements. As in other mixed methods, we maintain the local approximation of the divergence (i.e., local mass conservation). In contrast, Galerkin finite element methods facilitate general element shapes at the cost of achieving only global mass conservation. Our method is shown to be as accurate as the standard mixed method for a large class of smooth meshes. On non-smooth meshes or with non-smooth coefficients one can add Lagrange multiplier pressure unknowns on certain element edges or faces. This enhanced cell-centered procedure recovers full accuracy, with little additional cost if the coefficients or mesh geometry are piece-wise smooth. Theoretical error estimates and numerical examples are given illustrating the accuracy and efficiency of the methods.

Key words. mixed finite element, finite difference, elliptic differential equation, tensor coefficient, error estimates, logically rectangular grid, unstructured mesh, hierarchical mesh

AMS(MOS) subject classifications. 65N06, 65N12, 65N15, 65N22, 65N30

1. Introduction.

We discuss numerical methods for solving a second order elliptic problem posed on a possibly irregular domain $\Omega \subset \mathbf{R}^d$, $d = 2$ or 3. The problem is to find $(\mathbf{u}, p)$ such that

$$\mathbf{u} = -K\nabla p \quad \text{in } \Omega, \tag{1.1a}$$

$$\alpha p + \nabla \cdot \mathbf{u} = f \quad \text{in } \Omega, \tag{1.1b}$$

$$p = g^D \quad \text{on } \Gamma^D, \tag{1.1c}$$

$$\mathbf{u} \cdot \nu = g^N \quad \text{on } \Gamma^N, \tag{1.1d}$$

where $\alpha \geq 0$, f, g^D, and g^N are smooth functions, K is a symmetric, positive definite second order tensor with smooth or perhaps piece-wise smooth components, ν is the

* This work was supported in part by the Department of Energy, the State of Texas Governor's Energy Office, and grants from the National Science Foundation. The third author was supported in part by an NSF Postdoctoral Fellowship.

† Center for Subsurface Modeling, Texas Institute for Computational and Applied Mathematics, The University of Texas at Austin, Taylor Hall 2.400, Austin, Texas 78712.

‡ Department of Mathematics, University of Texas at Austin.

§ Department of Aerospace Engineering and Engineering Mechanics, University of Texas at Austin.

¶ Department of Petroleum and Geosystems Engineering, University of Texas at Austin.

♣ Department of Computational and Applied Mathematics, Rice University, Houston, Texas 77251–1892.

outward unit normal vector on $\partial\Omega$, and $\partial\Omega$ is decomposed into Γ^D and Γ^N. For simplicity, assume $\Gamma^D \neq \emptyset$ or $\alpha > 0$ on $\bar{\Omega}$, so (1.1) has a unique solution.

We are interested in applications to flow in porous media, where p is the pressure, $\mathbf{u}$ is the velocity field, K is related to the permeability tensor, and α is related to the rock compressibility. In these applications, accurate velocity approximations are required, and it is desirable that the conservation principle (1.1b) be satisfied locally, element by element. This precludes the use of Galerkin finite element methods, which only satisfy (1.1b) globally. Mixed finite element methods [28, 6] satisfy (1.1b) locally. The standard mixed method can be applied to general elements and general coefficients at the cost of a computationally expensive saddle-point linear system. (For background on the standard mixed method, including convergence and superconvergence results, see [31, 28, 13, 24, 17, 15, 16]).

Many techniques have been developed for solving the saddle point systems that arise in the standard formulation [19, 18, 30, 11, 26, 10]. However, the saddle point problem can be avoided altogether by introducing additional Lagrange multiplier pressure unknowns on the boundaries of the elements [2]. This hybrid formulation allows one to eliminate the velocity and the original pressure unknowns from the system. A positive definite system results, but at the expense of greatly increasing the number of unknowns. For the lowest order Raviart-Thomas mixed space RT_0 [28, 25], the hybrid form reduces to a face-centered finite difference method for the Lagrange pressures, one for each edge (if $d = 2$) or face (if $d = 3$).

In flow in porous media applications such as petroleum reservoir simulation, mixed finite element methods disguised as cell-centered finite difference methods have been the standard approach for many years [27, 29]. The relationship between the mixed method on rectangular meshes and cell-centered finite differences was first established in [29] provided that K in (1.1) is a scalar or a diagonal matrix, and later for general tensor K in [1] for a variant of the mixed method, the "expanded mixed method" [34, 22, 7, 1], again provided that the mesh is rectangular. If one uses the RT_0 space and applies appropriate quadrature rules, the velocity unknowns can be eliminated and the method reduces to a positive definite, cell-centered finite difference method for the pressure p with a stencil of 9 points if $d = 2$ and 19 points if $d = 3$ (but only 5 or 7, respectively, if K is diagonal). This method achieves superconvergence at certain discrete points for both the pressure and velocity [32, 23, 33, 1], and the number of unknowns is reduced to the number of cells or elements (which is much less than the number of edges or faces).

In this paper, we derive a numerical method as efficient as cell-centered finite differences on rectangles, yet that accurately handles cases with a full tensor K, a discontinuous K, non-affine quadrilateral or hexahedral elements, triangular elements, and non-smooth hierarchical meshes. We present an appropriate, new, expanded mixed variational formulation in §2 and discretize it in §3. In §4 we construct basis functions on general shaped elements, which we apply to the expanded mixed method in §5. In §6 and §7 we use quadrature rules to obtain cell-centered finite difference methods on logically rectangular grids and triangular meshes. Our method allows one to easily extend an existing rectangle based code to handle tensors and quadrilaterals. We give convergence theorems in §8 and corresponding computational results in §9. In §10 and §11, we discuss the effects of non-smooth meshes and coefficients. These are handled accurately by using an enhancement of the cell-centered finite difference method

given by adding Lagrange multiplier pressures along the discontinuities. Finally we give some conclusions in the last section.

2. An expanded variational form. Let $L^2(R)$ denote the usual Sobolev space of square-integrable functions on a domain $R \subset \mathbf{R}^d$, $d = 2, 3$. We denote by $(\,\cdot\,,\,\cdot\,)_R$ and $\|\psi\|_{0,R} = (\psi,\psi)_R^{1/2}$ the $L^2(R)$ inner product and norm, respectively. Let $\langle\cdot,\cdot\rangle_{\partial R}$ be the $L^2(\partial R)$ inner product or duality pairing. Define

$$H(\mathrm{div}; R) = \{\mathbf{v} \in (L^2(R))^d : \nabla\cdot\mathbf{v} \in L^2(R)\}.$$

When $R = \Omega$, we may omit it in the definitions above.

The discrete schemes that we discuss for (1.1) may refer explicitly to internal boundaries of Ω (cf. [19]). Let Ω be partitioned into one or more subdomains Ω_i, and let $\Gamma^I = \cup_i \partial\Omega_i \backslash \partial\Omega$ be the union of the boundaries of the Ω_i internal to the domain. In §10, we will take the internal boundaries to be along discontinuities in K, as between rock strata within an aquifer, or along the boundaries of a multi-block mesh. Define

$$H^I(\mathrm{div}) = \{\mathbf{v} \in (L^2(\Omega))^d : \nabla\cdot\mathbf{v}|_{\Omega_i} \in L^2(\Omega_i)\}.$$

We introduce the following expanded mixed variational form of (1.1):

$$(G\mathbf{u},\tilde{\mathbf{v}}) = (GKG\tilde{\mathbf{u}},\tilde{\mathbf{v}}), \qquad \tilde{\mathbf{v}} \in (L^2(\Omega))^d, \tag{2.1a}$$

$$(G\tilde{\mathbf{u}},\mathbf{v}) - \sum_i (p, \nabla\cdot\mathbf{v})_{\Omega_i} = -\langle g^D, \mathbf{v}\cdot\nu\rangle_{\Gamma^D} - \sum_i \langle p, \mathbf{v}\cdot\nu\rangle_{\partial\Omega_i\backslash\Gamma^D}, \quad \mathbf{v} \in H^I(\mathrm{div}), \tag{2.1b}$$

$$(\alpha p, w) + \sum_i (\nabla\cdot\mathbf{u}, w)_{\Omega_i} = (f, w), \qquad w \in L^2(\Omega), \tag{2.1c}$$

$$\sum_i \langle \mathbf{u}\cdot\nu, \mu\rangle_{\partial\Omega_i\backslash\Gamma^D} = \langle g^N, \mu\rangle_{\Gamma^N}, \qquad \mu \in H^{1/2}(\Gamma^N \cup \Gamma^I). \tag{2.1d}$$

This is expanded from the standard mixed variational form in that we have introduced a symmetric positive definite tensor field G and an additional unknown

$$\tilde{\mathbf{u}} = -G^{-1}\nabla p, \tag{2.2}$$

that represents an "adjusted gradient". In the recently introduced expanded formulation [34, 22, 7, 1], G is the identity. If instead $G = K^{-1}$, $\tilde{\mathbf{u}} = \mathbf{u}$ and one recovers the standard mixed method formulation. Later we define G based on the local geometry.

3. An expanded mixed method. Let $\{\mathcal{E}_h\}_{h>0}$ be a regular family of finite element partitions of Ω [9], where h is the maximal element diameter, such that each element edge or face on the domain boundary is contained entirely within either Γ^D or Γ^N, and such that Γ^I is contained in the union of the boundaries of the elements.

Associate with $\mathcal{E}_h$ a mixed finite element space $V_h^I \times W_h \times \Lambda_h^{I,N} \subset H^I(\mathrm{div}) \times L^2(\Omega) \times L^2(\Gamma^I \cup \Gamma^N)$, for example, any of the spaces defined in [31, 28, 25, 5, 4, 3, 8]. Each vector function in V_h^I has continuous normal components on the edges or faces between elements not contained in Γ^I; the space has no continuity constraint on Γ^I. Moreover, $\Lambda_h^{I,N}$ is the space of Lagrange multipliers; these functions are defined in a piecewise discontinuous manner on $\Gamma^I \cup \Gamma^N$ such that on an element edge or face $e \subset \Gamma^I \cup \Gamma^N$, $\Lambda_h^{I,N}|_e = V_h^I|_e \cdot \nu$. We need an additional finite element space $\tilde{V}_h$ such

that $V_h^I \subseteq \tilde{V}_h \subseteq (L^2(\Omega))^d$; until §11, we will generally take $\tilde{V}_h = V_h^I$, for reasons described below.

In our version of the expanded mixed method, we seek $\mathbf{U} \in V_h^I$, $\tilde{\mathbf{U}} \in \tilde{V}_h$, $P \in W_h$, and $\lambda \in \Lambda_h^{I,N}$ satisfying

$$(G\mathbf{U}, \tilde{\mathbf{v}}) = (GKG\tilde{\mathbf{U}}, \tilde{\mathbf{v}}), \qquad \tilde{\mathbf{v}} \in \tilde{V}_h, \tag{3.1a}$$

$$\begin{aligned}(G\tilde{\mathbf{U}}, \mathbf{v}) - \sum_i (P, \nabla \cdot \mathbf{v})_{\Omega_i} \\ = -\langle g^D, \mathbf{v} \cdot \nu \rangle_{\Gamma^D} - \sum_i \langle \lambda, \mathbf{v} \cdot \nu \rangle_{\partial\Omega_i \setminus \Gamma^D}, \quad \mathbf{v} \in V_h^I,\end{aligned} \tag{3.1b}$$

$$(\alpha P, w) + \sum_i (\nabla \cdot \mathbf{U}, w)_{\Omega_i} = (f, w), \qquad w \in W_h, \tag{3.1c}$$

$$\sum_i \langle \mathbf{U} \cdot \nu, \mu \rangle_{\partial\Omega_i \setminus \Gamma^D} = \langle g^N, \mu \rangle_{\Gamma^N}, \qquad \mu \in \Lambda_h^{I,N}. \tag{3.1d}$$

We are interested in three special cases. First, if there is only one subdomain, then $\Gamma^I = \emptyset$, $V_h^I \subset H(\mathrm{div}; \Omega)$, and Lagrange multipliers are used only to implement Neumann boundary conditions. Second, if each Ω_i is itself a single element in the computational mesh, then Γ^I is the set of all internal element faces, and we have the full hybrid method with Lagrange multipliers on each face (cf. [2]). Third, we may partition Ω into subdomains of intermediate size for purposes of domain decomposition on parallel computers, or to capture regions of smoothness in the coefficient K or in the mesh, so that we need put Lagrange multipliers only on subdomain boundaries (cf. [19]).

By choosing standard bases for the mixed finite element spaces, we reduce (3.1) to a symmetric linear system of the form

$$\begin{pmatrix} A_1 & -A_2 & 0 & 0 \\ -A_2^T & 0 & B^T & -C \\ 0 & B & D & 0 \\ 0 & -C^T & 0 & 0 \end{pmatrix} \begin{pmatrix} \check{\tilde{U}} \\ \check{U} \\ \check{P} \\ \check{\lambda} \end{pmatrix} = \begin{pmatrix} 0 \\ \check{g}^D \\ \check{f} \\ -\check{g}^N \end{pmatrix}, \tag{3.2}$$

where, in particular,

$$A_{1,ij} = (GKG\tilde{\mathbf{v}}_i, \tilde{\mathbf{v}}_j), \tag{3.3}$$

$$A_{2,ij} = (G\mathbf{v}_i, \tilde{\mathbf{v}}_j), \tag{3.4}$$

and $\{\mathbf{v}_i\}$ and $\{\tilde{\mathbf{v}}_i\}$ are bases for V_h^I and $\tilde{V}_h$, respectively. This system is an indefinite saddle-point problem, and it is quite large.

If $V_h^I = \tilde{V}_h$, then A_2 is square, symmetric, and invertible. In that case, the size of the linear system can be reduced by eliminating

$$\check{U} = A_2^{-1} A_1 \check{\tilde{U}}, \tag{3.5}$$

$$\check{\tilde{U}} = A_2^{-1}(B^T \check{P} - C\check{\lambda} - \check{g}^D), \tag{3.6}$$

to obtain the Shur complement system

$$(\mathcal{B} A_2^{-1} A_1 A_2^{-1} \mathcal{B}^T + \mathcal{D}) \begin{pmatrix} \check{P} \\ \check{\lambda} \end{pmatrix} = \begin{pmatrix} \check{f} \\ -\check{g}^N \end{pmatrix} + (\mathcal{B} A_2^{-1} A_1 A_2^{-1}) \check{g}^D, \tag{3.7}$$

where $\mathcal{B} = \begin{pmatrix} B \\ -C^T \end{pmatrix}$ and $\mathcal{D} = \begin{pmatrix} D & 0 \\ 0 & 0 \end{pmatrix}$. This system is symmetric, positive definite, and relatively small. Unfortunately, although A_2 is sparse, A_2^{-1} may not be. If it is not, an iterative solution will require 4 matrix-vector multiplies and 2 solutions of linear systems of the form $A_2 x = b$ (or only one such solution if A_1 is diagonal). That is, we need inner iterations within our overall iterative solution, which can become expensive. If A_2 could be made diagonal (through a careful choice of mixed finite element spaces and possibly through additional approximations), the cost of applying an iterative procedure to the solution of the linear system would be greatly reduced.

In the hybrid method where each Ω_i is a single element, A_2 is element-wise block diagonal and therefore easily inverted, although the resulting system is relatively large.

In the special case of RT_0 spaces, a single subdomain, and rectangular elements, applying the trapezoidal (or "trapezoidal-midpoint" [29]) quadrature rule to (3.3) and (3.4) reduces A_2 to a diagonal matrix [29, 1]. The full matrix in (3.7) then becomes sparse. In fact, the method reduces to a cell-centered finite difference method, with only as many unknowns as elements (up to some additional unknowns near Γ^N and Γ^I). Moreover, the accuracy of the approximate solutions is not compromised [33, 1]. In this paper we remove the restriction to rectangular elements and a single subdomain. We begin by considering carefully the finite element spaces on irregularly shaped elements.

4. The mixed finite element spaces for general elements. Many mixed finite element spaces are known [31, 28, 25, 5, 4, 3, 8]. The ones we consider can be constructed on a unit sized standard, regular reference element $\hat{E}$: an equilateral triangle, regular simplex, square, cube, or regular prism. An affine map then gives the definition on any triangle, tetrahedra, rectangular parallelepiped, or prism. The construction of quadrilateral and hexahedral elements is more involved, and we review here the basic theory of Thomas [31]. We then generalize the mixed spaces, defined on $\hat{E}$, to curved elements.

For any element E, let $F_E : \mathbf{R}^d \to \mathbf{R}^d$ be a smooth (at least C^1) mapping such that $F_E(\hat{E}) = E$, and let F_E be globally invertible on $\hat{E}$. Denote by $DF(\hat{\mathbf{x}})$ the Jacobian matrix of F_E ($DF_{ij} = \partial F_i / \partial x_j$), and let

$$J(\hat{\mathbf{x}}) = |\det(DF(\hat{\mathbf{x}}))|.$$

For any scalar function $\hat{\varphi}(\hat{\mathbf{x}})$ on $\hat{E}$, let

$$\varphi(\mathbf{x}) = \mathcal{F}(\hat{\varphi})(\mathbf{x}) \equiv \hat{\varphi} \circ F_E^{-1}(\mathbf{x}). \tag{4.1}$$

To construct a subspace of $H(\mathrm{div}; \Omega_i)$, we need to preserve the normal components of vector valued functions across the boundaries of the elements. We use the Piola transformation (see [31, 6]): For any function $\hat{\mathbf{q}} \in (L^2(\hat{E}))^d$, define

$$\mathbf{q}(\mathbf{x}) = \mathcal{G}(\hat{\mathbf{q}})(\mathbf{x}) \equiv \left(\frac{1}{J} DF\, \hat{\mathbf{q}} \right) \circ F_E^{-1}(\mathbf{x}). \tag{4.2}$$

LEMMA 4.1.

$$
\begin{aligned}
(\mathbf{q}, \nabla\varphi)_E &= (\hat{\mathbf{q}}, \hat{\nabla}\hat{\varphi})_{\hat{E}}, && \varphi \in H^1(E),\ \mathbf{q} \in (L^2(E))^d,\\
(\varphi, \nabla\cdot\mathbf{q})_E &= (\hat{\varphi}, \hat{\nabla}\cdot\hat{\mathbf{q}})_{\hat{E}}, && \varphi \in L^2(E),\ \mathbf{q} \in H(\mathrm{div}; E),\\
\langle \mu, \mathbf{q}\cdot\nu\rangle_{\partial E} &= \langle \hat{\mu}, \hat{\mathbf{q}}\cdot\hat{\nu}\rangle_{\partial\hat{E}}, && \mathbf{q} \in H(\mathrm{div}; E),\ \mu \in H^{1/2}(\partial E).
\end{aligned}
$$

REMARK. The last equation states that the normal trace of an $H(\mathrm{div}; \hat{E})$ function is preserved in $H^{-1/2}(\partial\hat{E})$ after transformation by $\mathcal{G}$.

Let $\hat{V}_h(\hat{E}) \times \hat{W}_h(\hat{E}) \subset H(\mathrm{div}; \hat{E}) \times L^2(\hat{E})$ be any of our previously cited mixed spaces defined on the reference element $\hat{E}$, with $\hat{\Lambda}_h(\hat{e})$ the Lagrange multiplier space on edge or face $\hat{e} \subset \partial\hat{E}$. If $\mathcal{E}_h$ is a partition of Ω into elements of standard shape, Thomas [31] defined for each $E \in \mathcal{E}_h$ and $e \subset \partial E$,

$$V_h(E) = \{\mathbf{v} \in H(\mathrm{div}; E) : \mathbf{v} \overset{\mathcal{G}}{\longleftrightarrow} \hat{\mathbf{v}} \in \hat{V}_h(\hat{E})\}, \tag{4.3}$$

$$W_h(E) = \{w \in L^2(E) : w \overset{\mathcal{F}}{\longleftrightarrow} \hat{w} \in \hat{W}_h(\hat{E})\}, \tag{4.4}$$

$$\Lambda_h(e) = \{\mu \in L^2(e) : \mu \overset{\mathcal{F}}{\longleftrightarrow} \hat{\mu} \in \hat{\Lambda}_h(\hat{e})\}, \tag{4.5}$$

and then

$$V_h^I = \{\mathbf{v} : \mathbf{v} \in H^I(\mathrm{div}) \text{ and } \mathbf{v}|_E \in V_h(E),\ \forall E \in \mathcal{E}_h\}, \tag{4.6}$$

$$W_h = \{w \in L^2(\Omega) : w|_E \in W_h(E),\ \forall E \in \mathcal{E}_h\}, \tag{4.7}$$

$$\Lambda_h^{I,N} = \{\mu \in L^2(\Gamma^I \cup \Gamma^N) : \mu|_e \in \Lambda_h(e),\ \forall \text{ edge or face } e \text{ of } \mathcal{E}_h \text{ in } \Gamma^I \cup \Gamma^N\}. \tag{4.8}$$

We also define $\tilde{V}_h$ from $\hat{\tilde{V}}_h$ using (4.2) as in (4.3) and (4.6).

We generalize the mixed spaces to curved elements in a straightforward way. Let $\hat{\Omega}$ be our computational reference domain and let

$$F : \mathbf{R}^d \to \mathbf{R}^d, \quad F(\hat{\Omega}) = \Omega,$$

be a smooth (at least C^2) invertible map. Let $\hat{\mathcal{E}}_h$ be a regular family of partitions of $\hat{\Omega}$ into standard shaped elements. This gives a mesh on $\hat{\Omega}$, and its image by F is a curved mesh $\mathcal{E}_h$ on Ω. Let $\hat{V}_h^I \times \hat{W}_h \times \hat{\Lambda}_h^{I,N}$ be any of the usual mixed spaces defined over $\hat{\mathcal{E}}_h$. The mixed spaces on $\mathcal{E}_h$ are defined by (4.3)–(4.8).

5. Application to general geometry. We use F to map the problem (1.1) and its mixed approximation on Ω to $\hat{\Omega}$ using the isomorphisms $\mathcal{F}$ and $\mathcal{G}$, defined in §4, for mapping scalar and vector functions, respectively.

For the expanded method, we make a careful choice of G in (2.2) to simplify the interaction of the basis functions in (3.4) on the computational domain $\hat{\Omega}$. Define

$$G(F(\hat{\mathbf{x}})) = \big(J(DF^{-1})^T DF^{-1}\big)(\hat{\mathbf{x}}). \tag{5.1}$$

Note that G is symmetric and positive definite. Then,

$$G\mathbf{v}\cdot\tilde{\mathbf{v}} = J(DF^{-1})^T DF^{-1}\left(\frac{1}{J}DF\,\hat{\mathbf{v}}\right)\cdot\left(\frac{1}{J}DF\,\hat{\tilde{\mathbf{v}}}\right) = \frac{1}{J}\,\hat{\mathbf{v}}\cdot\hat{\tilde{\mathbf{v}}}, \quad \mathbf{v} \in V_h^I, \tilde{\mathbf{v}} \in \tilde{V}_h. \tag{5.2}$$

We obtain the following mixed formulation on the reference domain. Find $\hat{\mathbf{U}} \in \hat{V}_h^I$, $\hat{\tilde{\mathbf{U}}} \in \hat{\tilde{V}}_h$, $\hat{P} \in \hat{W}_h$, and $\hat{\lambda} \in \hat{\Lambda}_h^{I,N}$ such that

$$(\hat{\mathbf{U}}, \hat{\tilde{\mathbf{v}}})_{\hat{\Omega}} = (\mathcal{K}\hat{\tilde{\mathbf{U}}}, \hat{\tilde{\mathbf{v}}})_{\hat{\Omega}}, \qquad \hat{\tilde{\mathbf{v}}} \in \hat{\tilde{V}}_h, \tag{5.3a}$$

$$\begin{aligned}(\hat{\tilde{\mathbf{U}}}, \hat{\mathbf{v}})_{\hat{\Omega}} - \sum_i (\hat{P}, \hat{\nabla} \cdot \hat{\mathbf{v}})_{\hat{\Omega}_i} \\ = -\langle \hat{g}^D, \hat{\mathbf{v}} \cdot \hat{\nu} \rangle_{\hat{\Gamma}^D} - \sum_i \langle \hat{\lambda}, \hat{\mathbf{v}} \cdot \hat{\nu} \rangle_{\partial \hat{\Omega}_i \setminus \hat{\Gamma}^D}, \quad \hat{\mathbf{v}} \in \hat{V}_h^I,\end{aligned} \tag{5.3b}$$

$$(J\hat{\alpha}\hat{P}, \hat{w})_{\hat{\Omega}} + \sum_i (\hat{\nabla} \cdot \hat{\mathbf{U}}, \hat{w})_{\hat{\Omega}_i} = (J\hat{f}, \hat{w}), \qquad \hat{w} \in \hat{W}_h, \tag{5.3c}$$

$$\sum_i \langle \hat{\mathbf{U}} \cdot \hat{\nu}, \hat{\mu} \rangle_{\partial \hat{\Omega}_i \setminus \hat{\Gamma}^D} = \langle J_{\hat{\nu}} \hat{g}^N, \hat{\mu} \rangle_{\hat{\Gamma}^N}, \qquad \hat{\mu} \in \hat{\Lambda}_h^{I,N}, \tag{5.3d}$$

where the tensor K has been modified to

$$\mathcal{K} = JDF^{-1} K (DF^{-1})^T, \tag{5.4}$$

and $J_{\hat{\nu}}(\hat{\mathbf{x}}) = J(\hat{\mathbf{x}}) |(DF^{-1})^T \hat{\nu}|$. Note that $\hat{V}_h^I \times \hat{W}_h \times \hat{\Lambda}_h^{I,N}$ are the usual mixed spaces on reference elements, and $\hat{\tilde{V}}_h = \mathcal{F}^{-1}(\tilde{V}_h)$. Also, there are no coefficients in the L^2-vector inner-products on the left side of the first two equations.

6. Enhanced Cell-centered finite differences on logically rectangular grids. In this section we consider the RT_0 [28, 31, 25] spaces on curved but logically rectangular grids generated by taking a rectangular computational domain $\hat{\Omega}$, imposing on it a rectangular grid, and mapping it to Ω by the function F. We recall the definition of the RT_0 space in three space dimensions:

$$W_h = \{ w : w|_E \text{ is constant } \forall E \in \mathcal{E}_h \}, \tag{6.1}$$

$$\Lambda_h^{I,N} = \{ \mu : \mu|_e \text{ is constant on each face } e \subset \partial E \cap (\Gamma^I \cup \Gamma^N) \ \forall E \in \mathcal{E}_h \}, \tag{6.2}$$

and V_h^I is defined by (4.6) from

$$\begin{aligned}V_h(E) = \{ \mathbf{v} = (v_1, v_2, v_3) : v_\ell = a_\ell + b_\ell x_\ell, \\ \ell = 1, 2, 3, \text{ for some 6 constants } a_\ell \text{ and } b_\ell \}\end{aligned} \tag{6.3}$$

(i.e., for $\mathbf{v} \in V_h^I$, $v_\ell|_E$ is linear in the ℓ-direction, constant in the other two directions, and v_ℓ itself is continuous in the ℓth direction, except across Γ^I). In its standard nodal basis, W_h is defined at the element or cell centers, $\Lambda_h^{I,N}$ is defined at the appropriate face centers, and V_h^I is defined at the face centers, doubly defined along Γ^I. A similar definition gives RT_0 if $d = 2$.

For geometrically irregular domains, the transformed coefficient $\mathcal{K}$ of (5.4) is necessarily a full tensor except in trivial cases. Because of our choice (5.1) of G, if there is a single subdomain boundary, the expanded problem on the computational grid (5.3) is the same as that analyzed in [1]. It takes $\tilde{V}_h = V_h^I$ and (5.3c)–(5.3d)

combined with

$$(\hat{\mathbf{U}},\hat{\tilde{\mathbf{v}}})_{\hat{\Omega},\mathbf{T}} = (\mathcal{K}\hat{\tilde{\mathbf{U}}},\hat{\tilde{\mathbf{v}}})_{\hat{\Omega},\mathbf{T}}, \qquad \hat{\tilde{\mathbf{v}}} \in \hat{\tilde{V}}_h = \hat{V}_h^I, \tag{6.4a}$$

$$\begin{aligned}(\hat{\tilde{\mathbf{U}}},\hat{\mathbf{v}})_{\hat{\Omega},\mathbf{T}} - \sum_i (\hat{P},\hat{\nabla}\cdot\hat{\mathbf{v}})_{\hat{\Omega}_i} \\ = -\langle \hat{g}^D, \hat{\mathbf{v}}\cdot\hat{\nu}\rangle_{\hat{\Gamma}^D} - \sum_i \langle \hat{\lambda}, \hat{\mathbf{v}}\cdot\hat{\nu}\rangle_{\partial\Omega_i\setminus\hat{\Gamma}^D}, \quad \hat{\mathbf{v}} \in \hat{V}_h^I,\end{aligned} \tag{6.4b}$$

where $(\cdot\,,\cdot)_{R,\mathbf{T}}$ denotes the trapezoidal quadrature rule applied to the inner-product integral over R. By the nodal definition of RT_0, the trapezoidal quadrature rule diagonalizes A_2 in (3.4) on the computational domain:

$$\hat{A}_{2,ij} = (\hat{\mathbf{v}}_i,\hat{\mathbf{v}}_j)_{\hat{\Omega},\mathbf{T}} = \hat{C}_{ij}\delta_{ij}, \tag{6.5}$$

where $\hat{C}_{ij}$ is a constant related to the mesh size. With a single subdomain, the method reduces to cell-centered finite differences with a stencil (see [1]) of 19 points if $d = 3$ and 9 points if $d = 2$ for $\hat{P}$ in the Shur complement form of (3.2), i.e., (3.7). This is an approximation to the expanded mixed method. When multiple subdomains are present, we call the method the enhanced cell-centered finite difference method, since it is enhanced with face-centered variables along Γ^I.

The approximation of our problem (1.1) is now relatively simple. A preprocessing step can be done to transform the coefficients (by multiplication by either J or $J_{\hat{p}}$, or by the tensor transformation (5.4)). Then (6.4), (5.3c)–(5.3d) is solved as an entirely rectangular problem. Finally, (4.1)–(4.2) (i.e., $\mathcal{F}$ and $\mathcal{G}$) map the results $\hat{P}$ and $\hat{\mathbf{U}}$ back to P and $\mathbf{U}$ on the physical domain as approximations to p and $\mathbf{u}$.

7. Enhanced Cell-centered finite differences on triangles. In this section we consider $d = 2$ and a triangular mesh. Actually, on $\hat{\Omega}$, take a grid $\hat{\mathcal{E}}_h$ of equilateral triangles. As in the logically rectangular case, we take $\tilde{V}_h = V_h^I$ and seek a quadrature rule that diagonalizes A_2 of (3.4). The triangular RT_0 spaces are defined as in (6.1)–(6.3) above, with now E a triangle and (6.3) replaced by

$$\begin{aligned}V_h(E) = \big\{\mathbf{v} = (v_1,v_2) : v_\ell = a_\ell + bx_\ell, \\ \ell = 1,2, \text{ for some 3 constants } a_\ell \text{ and } b\big\}.\end{aligned} \tag{7.1}$$

Let $\hat{T}$ represent the standard reference equilateral triangle with vertices at $(-1,0)$, $(1,0)$, and $(0,\sqrt{3})$. Here let $\hat{\mathbf{v}}^k$ be the basis function of $\hat{V}_h(\hat{T})$ associated with edge k, denoted by $\hat{e}_k$, $k = 1,2,3$. We define our quadrature rule $\hat{Q}_{\hat{T}}(\psi)$ on $\hat{T}$ such that it is exact for polynomials of degree one, and $\hat{Q}_{\hat{T}}(\hat{\mathbf{v}}^k\cdot\hat{\mathbf{v}}^\ell) = 0$ for $k \neq \ell$:

$$\hat{Q}_{\hat{T}}(\psi) = \frac{\sqrt{3}}{6}\left[\psi(-1,0) + \psi(1,0) + \psi(0,\sqrt{3}) + 3\psi\left(0,\frac{\sqrt{3}}{3}\right)\right]. \tag{7.2}$$

The required properties follow easily from the definition of RT_0. (Incidentally, this rule is second order accurate if the 6 is replaced by 12 and the 3 in front of the last term is replaced by 9, but then orthogonality is lost.) There is no corresponding rule on a non-equilateral triangle; it is necessary to consider the mapping to the reference element.

The scheme is now (5.3c)–(5.3d) combined with

$$\text{(7.3a)} \qquad \sum_{\hat{T}\in\hat{\mathcal{E}}_h} \hat{Q}_{\hat{T}}(\hat{\mathbf{U}}\cdot\hat{\tilde{\mathbf{v}}}) = (\mathcal{K}\hat{\tilde{\mathbf{U}}},\hat{\tilde{\mathbf{v}}})_{\hat{\Omega}}, \qquad \hat{\tilde{\mathbf{v}}}\in\hat{\tilde{V}}_h = \hat{V}_h^I,$$

$$\text{(7.3b)} \qquad \sum_{\hat{T}\in\hat{\mathcal{E}}_h} \hat{Q}_{\hat{T}}(\hat{\tilde{\mathbf{U}}}\cdot\hat{\mathbf{v}}) - \sum_i (\hat{P},\hat{\nabla}\cdot\hat{\mathbf{v}})_{\hat{\Omega}_i}$$
$$= -\langle\hat{g}^D,\hat{\mathbf{v}}\cdot\hat{\nu}\rangle_{\hat{\Gamma}^D} - \sum_i \langle\hat{\lambda},\hat{\mathbf{v}}\cdot\hat{\nu}\rangle_{\partial\Omega_i\setminus\hat{\Gamma}^D}, \quad \hat{\mathbf{v}}\in\hat{V}_h^I.$$

Since the two integrals above approximated by quadrature are diagonal, in the interior of a subdomain the method gives a 10 point cell-centered finite difference stencil for $\hat{P}$ in the Shur complement form of (3.2), as shown in Fig. 7.1.

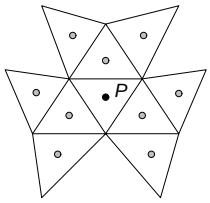

Fig. 7.1. Finite difference stencil for P.

The approximation of our problem (1.1) can be solved as in the logically rectangular case (transform coefficients, solve the transformed problem, and map the solution back to the physical domain). Since now the computational mesh is not orthogonal, it may be simpler in practice to compute this approximation to the expanded mixed method (3.1) directly on the physical mesh. We approximate on each triangle $T\in\mathcal{E}_h$ in the integral evaluation routine

$$\text{(7.4)} \qquad (G\mathbf{v},\tilde{\mathbf{v}})_T = (\hat{\mathbf{v}},\hat{\tilde{\mathbf{v}}})_{\hat{T}} \approx \hat{Q}_{\hat{T}}(\hat{\mathbf{v}},\hat{\tilde{\mathbf{v}}}).$$

In three dimensions, regular tetrahedra do not fill space, so there is no regular computational mesh. However, we can proceed in a local sense. Take a tetrahedral mesh on Ω, such that each element $E\in\mathcal{E}_h$ is the image by F_E of the standard reference regular tetrahedron $\hat{T}$ with vertices at $\mathbf{x}^1=(-1,0,0)$, $\mathbf{x}^2=(1,0,0)$, $\mathbf{x}^3=(0,\sqrt{3},0)$, and $\mathbf{x}^4=(0,\sqrt{3}/3,2\sqrt{6}/3)$. Proceeding element-by-element, we diagonalize A_2 with the first order approximation:

$$\text{(7.5)} \quad \hat{Q}_{\hat{T}}(\psi) = \frac{\sqrt{2}}{18}\left[\psi(\mathbf{x}^1)+\psi(\mathbf{x}^2)+\psi(\mathbf{x}^3)+\psi(\mathbf{x}^4)+8\psi\left(\frac{\mathbf{x}^1+\mathbf{x}^2+\mathbf{x}^3+\mathbf{x}^4}{4}\right)\right].$$

In this case, the stencil has at most seventeen nonzero entries. There is a problem with the accuracy of this method, and we will return to it in §10.

8. Some convergence results. With the notable exception of the work of Thomas [31], most of the known convergence estimates apply only to affine elements and special boundary elements. Recall that affine elements are the image by an affine map of an equilateral triangle, square, cube, regular simplex, or regular prism (i.e., the standard, regular reference elements), and that quadrilaterals and hexahedra are not affine elements. One feature of these elements is that $\nabla\cdot V_h^I = W_h$. For the

curved elements defined in §4, note that Lemma 4.1 and the fact that $(\varphi, \nabla \cdot \mathbf{u})_E = (J\hat{\varphi}, \widehat{\nabla \cdot \mathbf{u}})_{\hat{E}}$ implies

$$\nabla \cdot \mathbf{u}(\mathbf{x}) = \widehat{\nabla \cdot \mathbf{u}} \circ F^{-1}(\mathbf{x}) = \left(\frac{1}{J}\hat{\nabla} \cdot \hat{\mathbf{u}}\right) \circ F^{-1}(\mathbf{x}); \tag{8.1}$$

thus, in general $\nabla \cdot V_h^I \neq W_h$, unless the map F is piecewise affine. In this section we present some convergence results and extend them to the curved element case.

Let $W^{j,q}(\Omega)$ be the usual Sobolev space of j-times differentiable functions in $L^q(\Omega)$, with the norm $\| \cdot \|_{j,q}$. Let $H^j(\Omega) = W^{j,2}$ with its norm $\| \cdot \|_j$. We describe the approximation properties of the mixed finite element spaces by l_V and l_W, where

$$\min_{\mathbf{v} \in V_h} \|\mathbf{q} - \mathbf{v}\|_0 \leq C \|\mathbf{q}\|_l \, h^l, \qquad 1 \leq l \leq l_V, \tag{8.2}$$

$$\min_{w \in W_h} \|\psi - w\|_0 \leq C \|\psi\|_l \, h^l, \qquad 0 \leq l \leq l_W, \tag{8.3}$$

$$\min_{\mathbf{v} \in V_h} \|\nabla \cdot (\mathbf{q} - \mathbf{v})\|_0 \leq C \|\nabla \cdot \mathbf{q}\|_l \, h^l, \quad 0 \leq l \leq l_W. \tag{8.4}$$

For the spaces of [28, 31, 25, 4], $l_W = l_V$, while for the spaces of [5, 3], $l_W = l_V - 1$. The spaces of [8] are a generalization of these other spaces on prisms.

To quantify dependencies on the mapping $F \in (W^{\ell,\infty}(\hat{\Omega}))^{d \times d}$, throughout this section, $C_{F,\ell}$ will denote a generic positive constant that is independent of the discretization parameter h, but may depend on $\hat{\Omega}$, $\|\alpha\|_{0,\infty}$, $\|K\|_{0,\infty}$, $\|K^{-1}\|_{0,\infty}$, and also on F but only through $\|F\|_{\ell,\infty}$, $\|F^{-1}\|_{\ell,\infty}$, $\|J\|_{0,\infty}$, $\|J^{-1}\|_{0,\infty}$, $\|DF\|_{0,\infty}$, and $\|DF^{-1}\|_{0,\infty}$. To describe the superconvergence results for the pressure, denote the $L^2(\Omega)$-projection operator onto W_h by $\mathcal{P}_W$; that is, for $\psi \in L^2(\Omega)$, we define $\mathcal{P}_W \psi$ by

$$(\psi - \mathcal{P}_W \psi, w) = 0, \quad w \in W_h.$$

THEOREM 8.1. *For the expanded mixed method* (3.1) *with* $F = I$ *and either* $G = I$ *or* $G = K^{-1}$ *on affine (and special boundary) elements or with* G *defined by* (5.1) *on curved elements,*

$$\|\mathbf{u} - \mathbf{U}\|_0 + \|\tilde{\mathbf{u}} - \tilde{\mathbf{U}}\|_0 \leq C_{F,\ell+1}(\|p\|_{l+1} + \|\mathbf{u}\|_l) \, h^l, \quad 1 \leq l \leq l_V, \tag{8.5}$$

$$\|p - P\|_0 \leq C_{F,\ell+1}(\|p\|_{l+1} + \|\mathbf{u}\|_l) \, h^l, \qquad 1 \leq l \leq l_W, \tag{8.6}$$

$$\|\nabla \cdot (\mathbf{u} - \mathbf{U})\|_0 \leq C_{F,\ell+1}(\|p - P\|_0 + \|\nabla \cdot \mathbf{u}\|_l \, h^l), \quad 0 \leq l \leq l_W. \tag{8.7}$$

Moreover, if $l_W = l_V$,

$$\|\mathcal{P}_W p - P\|_0 \leq C_{F,\ell+3/2}(\|p\|_{l+1} + \|\nabla \cdot \mathbf{u}\|_l + \|\mathbf{u}\|_{l+1/2}) \, h^{l+1}, \quad 1 \leq l \leq l_W, \tag{8.8}$$

and, if $l_W < l_V$,

$$\begin{aligned} \|\mathcal{P}_W p - P\|_0 \leq \big\{ & C_{F,\ell_1+1}(\|p\|_{l_1+1} + \|\mathbf{u}\|_{l_1} + \|\nabla \cdot \mathbf{u}\|_{l_1}) \, h^{l_1 + \min\{l_W, 2\}} \\ & + C_{F,\ell_2+3/2}(\|p\|_{l_2+1} + \|\mathbf{u}\|_{l_2+1/2}) \, h^{l_2+1} \big\}, \quad 1 \leq l_1 \leq l_W, \ 1 \leq l_2 \leq l_V, \end{aligned} \tag{8.9}$$

where the $C_{F,s}$ *depend also on* $\|\alpha\|_{1,\infty}$ *and* $\|J\|_{1,\infty}$ *in* (8.8) *or if* $l_W < l_V$, *on* $\|K\|_{1,\infty}$, $\|DF\|_{1,\infty}$, *and* $\|DF^{-1}\|_{1,\infty}$ *in* (8.8)–(8.9), *and on* $\|\alpha\|_{2,\infty}$ *and* $\|J\|_{2,\infty}$ *in* (8.9).

Proof. When $F = I$, $G = I$ or $G = K^{-1}$, and the usual affine (or special boundary) elements are used, the theorem (with a straightforward modification for the lower order term and the boundary conditions) can be found in [31, 28, 13, 5, 3, 4, 8, 1, 7].

The results for curved elements follow from the case of the usual elements applied to the transformed problem (5.3), using relations (4.1), (4.2), and (8.1). □

REMARK. Other known estimates in H^{-s} and L^p norms for affine elements [13, 3, 4, 17, 1] can also be transformed for curved elements. If the grid is rectangular, Raviart-Thomas spaces [28, 31, 25] are used, and K is a diagonal matrix, we have also superconvergence in the standard mixed method for the velocity error in certain discrete norms [24, 15, 16]. However, since the map F introduces a non-diagonal transformation of K, these results do not carry over directly to curved elements.

REMARK. If multi-linear, quadrilateral and hexahedral elements are used, F is not continuous; however, we have approximation results because they hold element by element. If F is locally bilinear, then (see [31])

$$\|DF\|_{0,\infty} \le Ch^{-1} \quad \text{and} \quad \|DF\|_{j,\infty} \le Ch^{-2}, \quad j \ge 1,$$

and the results are non-optimal. However, for the Raviart-Thomas elements in two dimensions, Thomas [31] extracted somewhat sharper estimates for the standard mixed method. Similar results can be obtained for the expanded mixed method.

To describe the results for logically rectangular grids, we need some additional notation, given here in two dimensions for simplicity. Denote grid points on $\hat{\Omega}$ by

$$(\hat{x}_{i+1/2}, \hat{y}_{j+1/2}),$$

and then define

$$\hat{x}_i = \tfrac{1}{2}(\hat{x}_{i+1/2} + \hat{x}_{i-1/2}) \quad \text{and} \quad \hat{y}_j = \tfrac{1}{2}(\hat{y}_{j+1/2} + \hat{y}_{j-1/2}).$$

For any function $\hat{\psi}(\hat{x}, \hat{y})$, let $\hat{\psi}_{ij}$ denote $\hat{\psi}(\hat{x}_i, \hat{y}_j)$, let $\hat{\psi}_{i+1/2,j}$ denote $\hat{\psi}(\hat{x}_{i+1/2}, \hat{y}_j)$, etc., Similar definitions hold for functions and points without carets.

Let $(\,\cdot\,,\,\cdot\,)_{R,\mathbf{M}}$ denote an application of the midpoint quadrature rule to the $L^2(R)$ inner product on R with respect to $\mathcal{E}_h$. For $w \in L^2(\Omega) \cap C^0(\bar{\Omega})$ and $\mathbf{v} \in (L^2(\Omega))^d \cap (C^0(\bar{\Omega}))^d$ let

$$\|w\|^2_{\mathbf{M}} = (w, w)_{\mathbf{M}}, \quad \|\mathbf{v}\|^2_{\mathbf{TM}} = (\mathbf{v}, \mathbf{v})_{\mathbf{TM}}, \quad \text{and} \quad \|\mathbf{v}\|^2_{\mathbf{M}} = (\mathbf{v}, \mathbf{v})_{\mathbf{M}};$$

these can also be defined on W_h or $\tilde{V}_h$. On W_h and V_h^I, the first two are norms, and the third is a semi-norm. For $E = E_{ij} \in \mathcal{E}_h$, define

$$\|\mathbf{v}\|^2_{\nu,E} = \left[(\mathbf{v}\cdot\nu)^2_{i-1/2,j} + (\mathbf{v}\cdot\nu)^2_{i+1/2,j} + (\mathbf{v}\cdot\nu)^2_{i,j-1/2} + (\mathbf{v}\cdot\nu)^2_{i,j+1/2}\right]|E|,$$
$$\|\mathbf{v}\|^2_{\nu} = \sum_E \|\mathbf{v}\|^2_{\nu,E},$$

where ν is the unit normal vector to the edges of the elements; this is a norm on V_h^I.

The following definition concerning mesh refinement is needed for the next two results (cf. [1; Definition 5.2]).

DEFINITION 8.2. *For $\ell \ge 1$, an asymptotic family of meshes is said to be generated by a C^ℓ map if there is a fixed map F such that each mesh is an image by F of a mesh that is composed of standard, regular, reference elements. Here F must be in $C^\ell(\bar{\hat{\Omega}})$ with $J > 0$.*

THEOREM 8.3. *For the cell-centered finite difference method on a logically rectangular grid, if $p \in C^{3,1}(\bar{\Omega})$, $\mathbf{u} \in \left(C^1(\bar{\Omega}) \cap W^{2,\infty}(\Omega)\right)^d$, and $K \in \left(C^1(\bar{\Omega}) \cap W^{2,\infty}(\Omega)\right)^{d\times d}$,*

then there exists a constant $C_{F,3}$, independent of h but dependent on the solution, K, and F as indicated, such that

$$\|\mathbf{u}-\mathbf{U}\|_{\mathbf{M}}+\|\tilde{\mathbf{u}}-\tilde{\mathbf{U}}\|_{\mathbf{M}}\le C_{F,3}h^r, \tag{8.10}$$

$$\|\mathbf{u}-\mathbf{U}\|_{\nu}+\|\tilde{\mathbf{u}}-\tilde{\mathbf{U}}\|_{\nu}\le C_{F,3}h^r, \tag{8.11}$$

$$\|\nabla\cdot(\mathbf{u}-\mathbf{U})\|_{\mathbf{M}}\le C_{F,3}h^2, \tag{8.12}$$

$$\|p-P\|_{\mathbf{M}}\le C_{F,3}h^2, \tag{8.13}$$

where $r=2$ if $\mathcal{K}$ in (5.4) is diagonal and $\Gamma^D=\emptyset$ and $r=3/2$ otherwise.

The proof is given in the appendix.

REMARK. The above results imply L^2 superconvergence for the computed pressure, velocity, and its divergence at the midpoints of the elements. The normal component of the velocity at the midpoints of the edges or faces is also superconvergent. Moreover, full second order superconvergence of the velocities is obtained in the strict interior of the domain [1; Theorem 5.10].

THEOREM 8.4. *For the triangular cell-centered finite difference method, if the computational grid is generated by a C^3 map, then*

$$\|\mathbf{u}-\mathbf{U}\|_0+\|\tilde{\mathbf{u}}-\tilde{\mathbf{U}}\|_0\le C_{F,3}h, \tag{8.14}$$

$$\|p-P\|_0\le C_{F,3}h, \tag{8.15}$$

$$\|\nabla\cdot(\mathbf{u}-\mathbf{U})\|_0\le C_{F,3}h. \tag{8.16}$$

These results are new, and their proof is given in the appendix.

REMARK. Experimentally we find that for smooth problems p is $O(h^2)$ superconvergent at the centroids of the triangles. Moreover, on three-lines meshes, the normal fluxes are also $O(h^2)$ superconvergent [14].

9. Computational results. We present some numerical results that illustrate the theory by solving elliptic problems in two and three dimensions. The results come from two different computer codes, one implemented to solve the problem on a logically rectangular grid, and the other implemented to use more general meshes.

9.1. Logically rectangular. The logically rectangular code was developed initially as a rectangular code following the ideas of [1] to treat tensors. A preprocessor was added to modify the coefficients of the problem as described in §§5–6 above, and a postprocessor was added to transform the reference solution $(\hat{P},\hat{\mathbf{U}})$ to the solution $(P,\mathbf{U})$ on the physical domain.

In these examples, $\Gamma^I=\emptyset$ and the true domain Ω is defined as the image of the unit square under the smooth map

$$F\begin{pmatrix}\hat{x}\\ \hat{y}\end{pmatrix}=\begin{pmatrix}\hat{x}+\frac{1}{10}\cos(3\hat{y})\\ \hat{y}+\frac{1}{10}\sin(6\hat{x})\end{pmatrix}=\begin{pmatrix}x\\ y\end{pmatrix}.$$

A uniform, rectangular grid on $\hat{\Omega}$ maps to a curved grid on Ω. Derivatives of the map are evaluated numerically, using only the coordinates of the grid points. We test diagonal and full permeability tensors; however, the problem on the computational domain always has a full tensor (see (5.4)). The permeability is

$$K=K_D=\begin{pmatrix}10&0\\0&1\end{pmatrix}\quad\text{or}\quad K=K_F=\begin{pmatrix}(x+2)^2+y^2&\sin(xy)\\ \sin(xy)&1\end{pmatrix},$$

and the true solution is

$$p(x,y) = x^3 y + y^4 + \sin(x)\cos(y),$$

with f defined accordingly by (1.1), and (1.1c) or (1.1d) replaced by the proper boundary condition. The problem is shown in Figure 9.1.

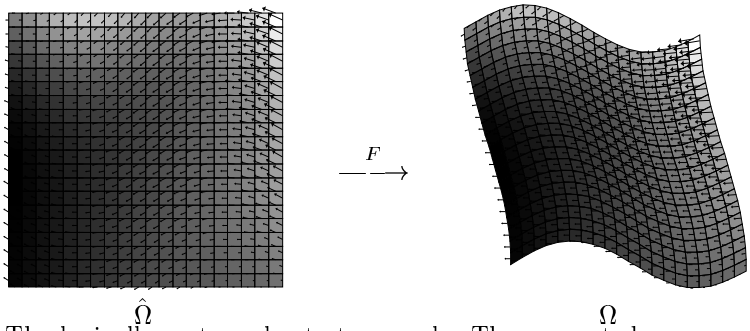

Fig. 9.1. The logically rectangular test example. The computed pressure and velocity are shown on both the computational and true domains for the case using K_F with Dirichlet boundary conditions.

Convergence rates for the test cases are given in Table 9.1. The rates were established by running the test case for 6 levels of grid refinement. We assume the error has the form Ch^α and compute C and α by a least squares fit to the data. As can be seen, the pressures and velocities are superconvergent to the true solution in the discrete norms. This verifies (8.13) and (8.10) with $r = 3/2$.

Table 9.1. Discrete norm convergence rates for the logically rectangular test example: $\|P - p\|_{\mathbf{M}} \le C_p\, h^{\alpha_p}$ and $\|\mathbf{U} - \mathbf{u}\|_{\mathbf{M}} \le C_u\, h^{\alpha_u}$.

Tensor	Boundary Condition	C_p	α_p	C_u	α_u
K_D	Dirichlet	0.417	2.260	0.588	1.659
K_D	Neumann	7.380	2.138	0.466	1.633
K_F	Dirichlet	0.435	2.205	0.611	1.710
K_F	Neumann	10.09	2.130	0.648	1.754

9.2. General meshes. The second code [20] is written in C++ for flexibility and implements a collection of mixed method formulations on two and three dimensional meshes composed of triangular, quadrilateral, tetrahedral, and hexahedral elements. This code operates element-by-element, and thus we approximate the map F locally by affine or bi/tri-linear mappings, as mentioned in §7.

We examined a large suite of test problems. In each case the boundary conditions and the forcing term were constructed to match the prescribed solution. We report in detail on a typical case and then summarize the results from the full test suite.

A typical case. Among the domains considered was that shown in Figure 9.2. This figure illustrates the initial decomposition of the domain into elements. Cubic splines, were used to describe the mesh and all of its refinements. The resulting family of meshes is smooth according to Definition 8.2.

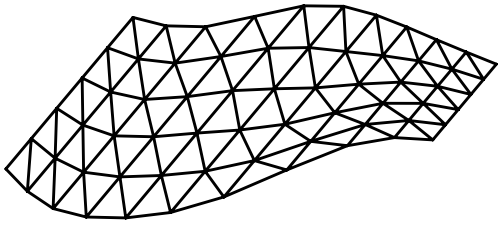

Fig. 9.2. The mesh for a typical example.

In Tables 9.2 we give detailed results for a test problem using Dirichlet boundary conditions,

$$K = \begin{pmatrix} 1 & 0.5 \\ 0.5 & 3 \end{pmatrix}, \tag{9.2.1}$$

and the analytic solution

$$\begin{aligned} p(x,y) = {} & 1 - 2.1\cos y + 3.1\cos 2y + 4\cos 3y \\ & + \cos x(5 + 6.2\cos y - 7.1\cos 2y + 8\cos 3y) \\ & + \cos 2x(9 - 10\cos y + 1.1\cos 2y + 12\cos 3y). \end{aligned} \tag{9.2.2}$$

We report errors in the pressure and velocity approximations for both the standard mixed method and the cell-centered finite difference approximation described in §5 and §7. As can be seen, the mixed and cell-centered methods are equally accurate, and converge at the expected rate.

Table 9.2. The errors in pressure and velocity for a typical example.

h	$\|P - p\|_{\mathbf{M}}$		$\|\mathbf{U} - \mathbf{u}\|_{\mathbf{M}}$	
	Mixed	Cell-centered	Mixed	Cell-centered
0.1	0.09366	0.09648	5.70698	5.92678
0.05	0.02577	0.02422	2.93120	2.97586
0.025	0.00668	0.00608	1.47783	1.48691
Rate	h^2	h^2	h	h

Summary of the test suite. We conducted approximately 200 experiments, varying the domain, the shape of the elements, the type of mesh refinement used, the boundary conditions, and the tensor K. We summarize results for $\Gamma^I = \emptyset$, smooth K, and smooth meshes that contain no tetrahedra. As we discuss in the next section, non-smoothness can degrade the accuracy.

In all smooth cases, the error in the pressure converged approximately like $O(h^2)$ for the standard mixed method and the cell-centered finite difference method. Similarly the error in the flux converged at least as well as $O(h)$ (grids of quadrilaterals or hexahedra perform better, as noted above).

Using a conjugate gradient solver with no preconditioning, the mixed method implemented as a saddle point problem took much longer than the unenhanced ($\Gamma^I = \emptyset$) cell-centered finite difference method (approximately 50 times longer on 2000 elements). On typical smooth problems, the unenhanced cell-centered method took approximately half as much CPU time as the face-centered hybrid method (where we take Γ^I as large as possible).

On rectangles, velocities are superconvergent at special points and can be postprocessed to yield second order accurate vector approximations everywhere [15]. A postprocessing scheme for triangular meshes developed by one of the authors [21] achieves a convergence rate for the postprocessed flux generally between $h^{1.5}$ and h^2, depending in part on the smoothness of the mesh refinement process. As shown in [14], on three-lines meshes, this and related postprocessing schemes recover second order accurate velocity fields, and they can be designed to conserve mass locally.

10. Non-smooth meshes and tensors. In this section we discuss the case in which $\mathcal{K}$ is not smooth, i.e., the mesh defined by F or the tensor K is not smooth. In practice, it is common to define F from the mesh points themselves; therefore, the mesh refinement process we use determines the smoothness of F. A mesh refinement process is called *hierarchical* if an initial coarse mesh is refined using a smooth refinement process (as in Definition 8.2) inside each of the original coarse elements; that is, the meshes form a smooth family within each coarse element, but not necessarily as a whole. In practice, most applications can use meshes and refinement schemes that are smooth or hierarchical.

We observed numerically that the accuracy of our unenhanced ($\Gamma^I = \emptyset$) cell-centered finite difference approach breaks down when $\mathcal{K}$ is not smooth. We demonstrate this by two simple but typical examples with $K = I$. First consider the two triangle, "non-smooth" mesh shown in Figure 10.1. Using Dirichlet boundary conditions and taking the true solution $p(x, y) = y$, the standard mixed method reproduces p at the centroids of the triangles and $\mathbf{u}$ exactly, as it must for $O(h)$ order accuracy. The unenhanced cell-centered finite difference method, in contrast, fails to compute either function correctly; for instance, it yields $P = 0.357$ instead of 0.333.

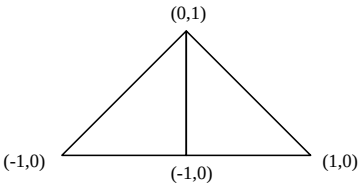

Fig. 10.1. A non-smooth mesh.

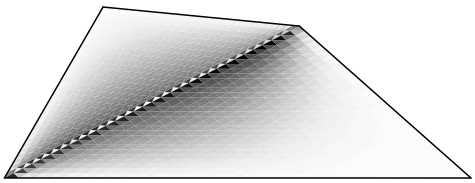

Fig. 10.2. Pressure error on a hierarchically refined mesh using unenhanced cell-centered finite differences.

Figure 10.2 shows the error $P - p$ for a second example on a hierarchical mesh constructed from applying uniform refinement to a coarse mesh of two dissimilar triangles. Within each coarse triangle, the mesh is smooth. Darker shades indicate larger errors. Clearly, it is the jump in DF across the central line that produces the main errors.

Since the normal component of $\hat{\mathbf{u}} = -\mathcal{K}\hat{\nabla}\hat{p}$ is continuous across an interface, $\hat{\tilde{\mathbf{u}}}$ must be discontinuous across any interface where $\mathcal{K}$ changes discontinuously. Since $\tilde{V}_h = V_h^I$ is discontinuous along Γ^I, we align the discontinuities in $\mathcal{K}$ along Γ^I. As we refine our mesh, we add Lagrange multipliers only along Γ^I. For the problem of Figure 10.1, this enhanced method gives the exact solution in the case of linear p.

A typical case. We illustrate the enhanced cell-centered finite difference method on a typical example posed on the domain and coarse hierarchical mesh shown in

Fig. 10.4. The domain is neither simply connected nor convex; moreover, we use both rectangles and triangles. The domain was refined uniformly by replacing each triangle or rectangle with 4 smaller but geometrically similar ones. The finest mesh had 2432 elements. The mapping F is clearly not smooth across edges of the coarse mesh (i.e., Γ^I), but it is smooth elsewhere.

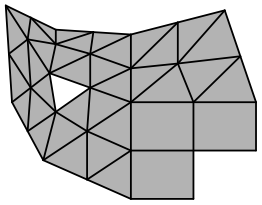

Fig. 10.4. A complex domain with a hierarchical mesh.

In Table 10.1, we give results for a test problem using Dirichlet boundary conditions, K defined by (9.2.1), and true solution (9.2.2). Indeed, the unenhanced method loses accuracy (about one half power of h in this example, but in other examples even more) in both pressure and flux as compared to the standard mixed method; however, there is no loss in accuracy for the enhanced cell-centered finite difference method. Moreover, if instead of this hierarchical refinement procedure, we use a smooth procedure on the domain, then the unenhanced cell-centered finite difference method achieves the same order of convergence as the other methods.

Table 10.1. The pressure error $\|P - p\|_{\mathbf{M}}$ and the velocity error $\|\mathbf{U} - \mathbf{u}\|_{\mathbf{M}}$ for a hierarchical example.

h	Mixed		Unenhanced Cell-centered		Enhanced Cell-centered	
	p	$\mathbf{u}$	p	$\mathbf{u}$	p	$\mathbf{u}$
0.16	0.39	6.0	0.48	9.3	0.59	6.4
0.08	0.11	3.1	0.12	5.9	0.11	3.5
0.04	0.029	1.5	0.043	3.7	0.026	1.6
0.02	0.0076	0.77	0.019	2.5	0.0062	0.80
Rate	h^2	h	$h^{1.4}$	$h^{0.6}$	h^2	h

Summary of the test suite. We also considered the enhanced method and non-smooth meshes in our test suite of the last section. For all methods, the convergence rate was approximately $O(h^2)$ for the error in the pressure, and at least as well as $O(h)$ for the error in the flux, except in the case of the unenhanced cell-centered finite difference method on non-smooth meshes. The enhanced method "corrects" the cell-centered method in the presence of non-smooth meshes or K. Moreover, on hierarchical meshes that have coarse blocks with smooth, logically rectangular meshes, the enhanced method achieved the usual superconvergence.

Recall that we used a conjugate gradient solver with no preconditioning. Generally, the enhanced method was somewhat slower than the hybrid method on coarse meshes, since in the hybrid method we can further eliminate the pressures and solve only for the Lagrange multipliers. By around four levels of mesh refinement, the two methods took the same amount of time to solve, since the enhanced method does

not need Lagrange multipliers on every edge. The enhanced method outperforms the hybrid method when additional refinement is used.

In many cases, Lagrange multipliers are needed only on the boundaries of a few elements, as between rock strata in an aquifer. A similar situation arises when applying the domain decomposition techniques described in [19], where Lagrange multipliers are introduced only on the element faces between subdomains. In the enhanced method, the multipliers are needed to preserve accuracy of the numerical solution; however, as a side effect, they can be used to introduce parallelism into the solution process. In [19, 18, 11, 10], various methods for solving such a system on parallel computers are developed and analyzed.

Tetrahedral meshes. We close this section by returning to tetrahedral meshes. Since regular tetrahedra do not fill space (whereas equilateral triangles do tile the plane), tetrahedral meshes unavoidably produce discontinuous $\mathcal{K}$ everywhere. Therefore, the cell-centered approach described in §7 requires Γ^I to include all element faces. Experimentally we observe that the enhanced method gives $O(h^2)$ accuracy for the pressure and $O(h)$ accuracy for the flux; however, since there are now Lagrange multiplier pressures on every face, this is not necessarily an improvement on the hybrid form of the standard mixed method.

11. An observation on the standard mixed method. Recall from the last section that when K is discontinuous, its discontinuities need to align with Γ^I and $\tilde{\mathbf{U}}$ must be discontinuous. Numerically, it has been observed that the standard mixed method ($G = K^{-1}$) performs well for discontinuous K even when $\Gamma^I = \emptyset$. In this case, as we now show, $\tilde{\mathbf{u}}$ is automatically approximated in a discontinuous space.

We rewrite the standard method in the following form. Find $\mathbf{U} \in V_h^I$, $\tilde{\mathbf{U}} \in \tilde{V}_h$, $P \in W_h$, and $\lambda \in \Lambda_h^{I,N}$ satisfying (3.1c)–(3.1d) and

$$(K^{-1}\mathbf{U}, \tilde{\mathbf{v}}) = (\tilde{\mathbf{U}}, \tilde{\mathbf{v}}) \qquad \tilde{\mathbf{v}} \in \tilde{V}_h, \tag{11.1a}$$

$$(\tilde{\mathbf{U}}, \mathbf{v}) - \sum_i (P, \nabla \cdot \mathbf{v})_{\Omega_i} = -\langle g^D, \mathbf{v} \cdot \nu \rangle_{\Gamma^D} - \sum_i \langle \lambda, \mathbf{v} \cdot \nu \rangle_{\partial\Omega_i \setminus \Gamma^D}, \quad \mathbf{v} \in V_h^I. \tag{11.1b}$$

Since $V_h^I \subset \tilde{V}_h$, these two equations combine to give the standard mixed method.

Suppose that $\tilde{V}_h$ is fully discontinuous (i.e., V_h^I when each element is a subdomain), take the orthogonal decomposition $\tilde{V}_h = V_h^I \oplus V_h^d$ with respect to the L^2 inner product, and expand

$$\tilde{\mathbf{U}} = \tilde{\mathbf{U}}^c + \tilde{\mathbf{U}}^d, \quad \tilde{\mathbf{U}}^c \in V_h^I \text{ and } \tilde{\mathbf{U}}^d \in V_h^d. \tag{11.2}$$

By orthogonality $\tilde{\mathbf{U}}^c$ replaces $\tilde{\mathbf{U}}$ in (11.1b); moreover, (11.1a) becomes the pair of equations

$$(K^{-1}\mathbf{U}, \tilde{\mathbf{v}}^c) = (\tilde{\mathbf{U}}^c, \tilde{\mathbf{v}}^c) \quad \tilde{\mathbf{v}}^c \in V_h^I, \tag{11.3a}$$

$$(K^{-1}\mathbf{U}, \tilde{\mathbf{v}}^d) = (\tilde{\mathbf{U}}^d, \tilde{\mathbf{v}}^d) \quad \tilde{\mathbf{v}}^d \in V_h^d. \tag{11.3b}$$

That is, the combination of (11.1b) and (11.3a), together with (3.1c)–(3.1d) forms the standard mixed method, solvable without reference to $\tilde{\mathbf{U}}$. Then (11.3a) defines the continuous part of $\tilde{\mathbf{U}}$, and (11.3b) defines the discontinuous part.

12. Some conclusions. The enhanced cell-centered finite difference method has been defined rigorously as a quadrature approximation of the expanded mixed method for general meshes of quadrilaterals, triangles, hexahedra, and tetrahedra. We saw both theoretically and computationally that if K is smooth, the unenhanced method is accurate and efficient on smooth meshes that are either logically rectangular or triangular with six triangles per interior vertex (it appears to be about twice as fast as competing methods). When K or the mesh is not smooth, the method loses accuracy, but the enhanced variant of the method does not. This enhanced method is more efficient than the hybrid form of the mixed method when the coarse subdomains are sufficiently refined so that the enhanced method uses many fewer Lagrange multiplier unknowns than the hybrid method, as when hierarchical meshes are used and/or when K is continuous over relatively large subdomains. Meshes of tetrahedral elements, however, are never smooth, so the unenhanced cell-centered finite difference method always loses accuracy and either the standard hybrid method or the enhanced method with Lagrange multipliers on every face should be used.

Appendix. Proofs of Theorems 8.3 and 8.4.

Proof of Theorem 8.3. The theorem is the transformation of the results of [1; Theorems 5.6 and 5.8]. To prove (8.10), we write

$$\|\mathbf{u}-\mathbf{U}\|_{\mathbf{M}}^2 = \left\|J^{-1}DF(\hat{\mathbf{u}}-\hat{\mathbf{U}})\right\|_{\mathbf{M}}^2 \le C\|\hat{\mathbf{u}}-\hat{\mathbf{U}}\|_{\mathbf{M}}^2.$$

Now, denoting $\mathbf{v}=(v^x,v^y)$ for $\mathbf{v}\in\mathbf{R}^2$,

$$\begin{aligned}\|\hat{u}^x-\hat{U}^x\|_{\mathbf{M}}^2 &= \sum_{\hat{E}}(\hat{u}^x-\hat{U}^x)_{ij}^2|\hat{E}|\\ &\le \sum_{\hat{E}}\left\{\frac{1}{2}\left[(\hat{u}^x-\hat{U}^x)_{i-1/2,j}+(\hat{u}^x-\hat{U}^x)_{i+1/2,j}\right]+C\hat{h}^2\right\}^2|\hat{E}|\\ &\le C\big(\|\hat{\mathbf{u}}-\hat{\mathbf{U}}\|_{\mathbf{T}}^2+\|\hat{\mathbf{u}}-\hat{\mathbf{U}}\|_{\mathbf{T}}\hat{h}^2+\hat{h}^4\big)\le C_{F,3}h^{2r},\end{aligned}$$

using a result from [1] for the last inequality. A similar bound for $\|\hat{u}^y-\hat{U}^y\|_{\mathbf{M}}$ completes the proof of (8.10). Estimate (8.11) follows trivially from the bound of $\|\hat{\mathbf{u}}-\hat{\mathbf{U}}\|_{\mathbf{T}}$ in [1] and the fact that $\mathbf{v}\cdot\nu = J_{\hat{\nu}}^{-1}\hat{\mathbf{v}}\cdot\hat{\nu}$ for $\mathbf{v}\in H(\mathrm{div};\Omega)$. To prove (8.12), we observe that $\hat{\nabla}\cdot\hat{\mathbf{U}}=\mathcal{P}_{\hat{W}}\hat{\nabla}\cdot\hat{\mathbf{u}}$ implies

$$\|\hat{\nabla}\cdot(\hat{\mathbf{u}}-\hat{\mathbf{U}})\|_{\mathbf{M}}\le C\|\hat{\nabla}\cdot\hat{\mathbf{u}}\|_2\hat{h}^2,$$

and, since $\widehat{\nabla\cdot\mathbf{u}} = J^{-1}\hat{\nabla}\cdot\hat{\mathbf{u}}$,

$$\|\nabla\cdot(\mathbf{u}-\mathbf{U})\|_{\mathbf{M}}\le C\|\hat{\nabla}\cdot(\hat{\mathbf{u}}-\hat{\mathbf{U}})\|_{\mathbf{M}}\le C_{F,3}h^2.$$

Finally, (8.13) follows from the estimate $\|\mathcal{P}_{\hat{W}}\hat{p}-\hat{P}\|_0\le C\hat{h}^2$ proven in [1]. □

Proof of Theorem 8.4. Assume the grid consists of equilateral triangles; the general case follows for curved elements as previously. Let

$$E_Q(\psi)=\sum_{T\in\mathcal{E}_h}\left[\int_T\psi\,dx-Q_T(\psi)\right]$$

denote the quadrature error. It is well known [12] that

$$|E_Q(\psi)| \le \sum_{T\in\mathcal{E}_h}\sum_{i,j}\int_T \left|\frac{\partial^2\psi}{\partial x_i\partial x_j}\right| dx\, h^2. \tag{A.1}$$

If $\mathbf{q}\in(H^2(\Omega))^d$ and $\mathbf{v}\in V_h$, then $\mathbf{v}$ is piecewise linear and

$$\begin{aligned}|E_Q(\mathbf{q}\cdot\mathbf{v})| &\le \sum_{T\in\mathcal{E}_h}\sum_{i,j}\int_T \left(\left|\frac{\partial^2\mathbf{q}}{\partial x_i\partial x_j}\cdot\mathbf{v}\right| + \left|\frac{\partial\mathbf{q}}{\partial x_i}\cdot\frac{\partial\mathbf{v}}{\partial x_j}\right|\right) dx\, h^2 \\ &\le C\|\mathbf{q}\|_2\,\|\mathbf{v}\|_1\,h^2 \le C\|\mathbf{q}\|_2\,\|\mathbf{v}\|_0\,h,\end{aligned} \tag{A.2}$$

by an inverse inequality [9].

Let $\mathcal{Q}_V : (L^2(\Omega))^d \to V_h$ denote the discrete $(L^2)^d$-projection operator defined by

$$\sum_{T\in\mathcal{E}_h} Q_T((\mathcal{Q}_V\mathbf{q}-\mathbf{q})\cdot\mathbf{v}) = 0, \quad \mathbf{v}\in V_h.$$

Clearly [12],

$$\|\mathcal{Q}_V\mathbf{q}-\mathbf{q}\|_0 \le C\|\mathbf{q}\|_1\,h. \tag{A.3}$$

Let $\Pi : (H^1(\Omega))^d \oplus V_h \to V_h$ be the flux preserving projection [28, 13] defined by

$$\sum_{E\in\mathcal{E}_h}\langle(\Pi\mathbf{q}-\mathbf{q})\cdot\nu,\mu\rangle_{\partial E} = 0, \quad \mu\in\Lambda_h.$$

By the divergence theorem, $(\nabla\cdot(\Pi\mathbf{q}-\mathbf{q}),w) = 0$ for $w\in W_h$, and approximation theory gives that

$$\|\Pi\mathbf{q}-\mathbf{q}\|_0 \le C\|\mathbf{q}\|_1\,h, \tag{A.4}$$

$$\|\nabla\cdot(\Pi\mathbf{q}-\mathbf{q})\|_0 \le C\|\nabla\cdot\mathbf{q}\|_1\,h. \tag{A.5}$$

Let $\mathcal{P}_\Lambda : L^2 \to \Lambda_h^N$ denote the L^2 projection defined by

$$\langle\mathcal{P}_\Lambda\varphi-\varphi,\mu\rangle_{\Gamma^N} = 0, \quad \mu\in\Lambda_h^N.$$

Easily, the L^2-projection errors are

$$\|\mathcal{P}_\Lambda\varphi-\varphi\|_{0,\Gamma^N} \le C\|\varphi\|_{H^1(\Gamma^N)}\,h, \tag{A.6}$$

$$\|\mathcal{P}_W\psi-\psi\|_0 \le C\|\psi\|_1\,h. \tag{A.7}$$

For simplicity assume α is constant; the variable coefficient case follows as a slight perturbation of the proof in the standard way. Subtracting the weak form of the problem, (2.1) with $G = I$, from the discrete method, (5.3c)–(5.3d), (7.3) with F

as the identity mapping, and inserting our projections operators gives

$$\text{(A.8a)}\qquad \sum_{T\in\mathcal{E}_h} Q_T((\mathbf{U}-\mathcal{Q}_V\mathbf{u})\cdot\tilde{\mathbf{v}}) = (K(\tilde{\mathbf{U}}-\tilde{\mathbf{u}}),\tilde{\mathbf{v}}) + E_Q(\mathbf{u}\cdot\tilde{\mathbf{v}}),\quad \tilde{\mathbf{v}}\in V_h,$$

$$\text{(A.8b)}\qquad \sum_{T\in\mathcal{E}_h} Q_T((\tilde{\mathbf{U}}-\mathcal{Q}_V\tilde{\mathbf{u}})\cdot\mathbf{v}) - (P-\mathcal{P}_W p,\nabla\cdot\mathbf{v}) = -\langle\lambda-\mathcal{P}_\Lambda p,\mathbf{v}\cdot\nu\rangle_{\Gamma^N} + E_Q(\tilde{\mathbf{u}}\cdot\mathbf{v}),\quad \mathbf{v}\in V_h,$$

$$\text{(A.8c)}\qquad (\alpha(P-\mathcal{P}_W p),w) + (\nabla\cdot(\mathbf{U}-\Pi\mathbf{u}),w) = 0,\quad w\in W_h,$$

$$\text{(A.8d)}\qquad \langle(\mathbf{U}-\Pi\mathbf{u})\cdot\nu,\mu\rangle_{\Gamma^N} = 0,\quad \mu\in\Lambda_h^N.$$

Take $\tilde{\mathbf{v}} = \tilde{\mathbf{U}}-\mathcal{Q}_V\tilde{\mathbf{u}}$, $\mathbf{v}=\mathbf{U}-\Pi\mathbf{u}$, $w=P-\mathcal{P}_W p$, and $\mu=\lambda-\mathcal{P}_\Lambda p$. A combination of the resulting equations yields

$$\begin{aligned}&(\alpha(P-\mathcal{P}_W p),P-\mathcal{P}_W p) + (K(\tilde{\mathbf{U}}-\mathcal{Q}_V\tilde{\mathbf{u}}),\tilde{\mathbf{U}}-\mathcal{Q}_V\tilde{\mathbf{u}})\\ &\quad = E_Q(\tilde{\mathbf{u}}\cdot(\mathbf{U}-\Pi\mathbf{u})) - E_Q(\mathbf{u}\cdot(\tilde{\mathbf{U}}-\mathcal{Q}_V\tilde{\mathbf{u}})) + (K(\tilde{\mathbf{u}}-\mathcal{Q}_V\tilde{\mathbf{u}}),\tilde{\mathbf{U}}-\mathcal{Q}_V\tilde{\mathbf{u}})\\ &\qquad + \sum_{T\in\mathcal{E}_h} Q_T((\tilde{\mathbf{U}}-\mathcal{Q}_V\tilde{\mathbf{u}})\cdot(\Pi\mathbf{u}-\mathcal{Q}_V\mathbf{u})).\end{aligned}$$

Since $\{\sum_{T\in\mathcal{E}_h} Q_T(\mathbf{v}\cdot\mathbf{v})\}^{1/2}$ is equivalent to the L^2-norm for $\mathbf{v}\in V_h$, standard estimates, (A.2), and (A.3) allow us to conclude that

$$\text{(A.9)}\qquad \begin{aligned}&\|\sqrt{\alpha}(P-\mathcal{P}_W p)\|_0 + \|\tilde{\mathbf{U}}-\mathcal{Q}_V\tilde{\mathbf{u}}\|_0\\ &\quad\le C\{\big[\|\tilde{\mathbf{u}}\|_2+\|\mathbf{u}\|_2\big]h + \|\Pi\mathbf{u}-\mathcal{Q}_V\mathbf{u}\|_0\} + \epsilon\|\mathbf{U}-\Pi\mathbf{u}\|_0\end{aligned}$$

for any $\epsilon>0$. If we take $\tilde{\mathbf{v}}=\mathbf{U}-\mathcal{Q}_V\mathbf{u}$ in (A.8a), then

$$\sum_{T\in\mathcal{E}_h} Q_T((\mathbf{U}-\mathcal{Q}_V\mathbf{u})\cdot(\mathbf{U}-\mathcal{Q}_V\mathbf{u})) = (K(\tilde{\mathbf{U}}-\tilde{\mathbf{u}}),\mathbf{U}-\mathcal{Q}_V\mathbf{u}) + E_Q(\mathbf{u}\cdot(\mathbf{U}-\mathcal{Q}_V\mathbf{u})),$$

and so

$$\text{(A.10)}\qquad \|\mathbf{U}-\mathcal{Q}_V\mathbf{u}\|_0 \le C\{\|\mathbf{u}\|_2\,h + \|\tilde{\mathbf{U}}-\tilde{\mathbf{u}}\|_0\}.$$

If $w=\nabla\cdot(\mathbf{U}-\Pi\mathbf{u})$ in (A.8c) and we manipulate the expression as above, then

$$\text{(A.11)}\qquad \|\nabla\cdot(\mathbf{U}-\Pi\mathbf{u})\|_0 \le C\|\sqrt{\alpha}(P-\mathcal{P}_W p)\|_0.$$

Finally, let $\mathbf{v}\in V_h$ be chosen such that for some ψ,

$$\begin{aligned}&\nabla\cdot\mathbf{v} = P-\mathcal{P}_W p-\mathcal{P}_W(\alpha\psi),\\ &\|\psi\|_0+\|\mathbf{v}\|_0 \le C\|P-\mathcal{P}_W p\|_0,\\ &\mathbf{v}\cdot\nu = 0\quad\text{on }\Gamma^N.\end{aligned}$$

Such a $\mathbf{v}$ exists [28, 13]; for example, solve

$$\begin{aligned}&\alpha\psi-\nabla\cdot K\nabla\psi = P-\mathcal{P}_W p && \text{in }\Omega,\\ &\psi = 0 && \text{on }\Gamma^D,\\ &K\nabla\psi\cdot\nu = 0 && \text{on }\Gamma^N,\end{aligned}$$

and then define $\mathbf{v} = -\Pi K \nabla \psi$ which preserves the normal flux and divergence of $-K\nabla\psi$ by the properties of Π, and bounds the norms by approximation and elliptic regularity theory. This $\mathbf{v}$ in (A.8b) gives

$$\|P - \mathcal{P}_W p\|_0 \le C\{\|\tilde{\mathbf{u}}\|_2\, h + \|\tilde{\mathbf{U}} - \mathcal{Q}_V \tilde{\mathbf{u}}\|_0 + \|\sqrt{\alpha}(P - \mathcal{P}_W p)\|_0\}. \tag{A.12}$$

The theorem follows from the approximation properties of the projections and (A.9)–(A.12). □

REFERENCES

[1] T. Arbogast, M. F. Wheeler, and I. Yotov, *Mixed finite elements for elliptic problems with tensor coefficients as cell-centered finite differences*, SIAM J. Numer. Anal., to appear.

[2] D. N. Arnold and F. Brezzi, *Mixed and nonconforming finite element methods: implementation, postprocessing and error estimates*, R.A.I.R.O. Modèl. Math. Anal. Numèr., 19 (1985), pp. 7–32.

[3] F. Brezzi, J. Douglas, Jr., R. Duràn, and M. Fortin, *Mixed finite elements for second order elliptic problems in three variables*, Numer. Math., 51 (1987), pp. 237-250.

[4] F. Brezzi, J. Douglas, Jr., M. Fortin, and L. D. Marini, *Efficient rectangular mixed finite elements in two and three space variables*, R.A.I.R.O. Modèl. Math. Anal. Numèr., 21 (1987), pp. 581-604.

[5] F. Brezzi, J. Douglas, Jr., and L. D. Marini, *Two families of mixed elements for second order elliptic problems*, Numer. Math., 88 (1985), pp. 217-235.

[6] F. Brezzi and M. Fortin, *Mixed and hybrid finite element methods*, Springer-Verlag, New York, 1991.

[7] Zhangxin Chen, *BDM mixed methods for a nonlinear elliptic problem*, J. Comp. Appl. Math., 53 (1994), pp. 207–223.

[8] Zhangxin Chen and J. Douglas, Jr., *Prismatic mixed finite elements for second order elliptic problems*, Calcolo, 26 (1989), pp. 135-148.

[9] P. G. Ciarlet, *The finite element method for elliptic problems*, North-Holland, New York, 1978.

[10] L. C. Cowsar, J. Mandel, and M. F. Wheeler, *Balancing domain decomposition for cell-centered finite differences*, Math. Comp., 64 (1995), pp. 989–1015.

[11] L. C. Cowsar, A. Weiser, and M. F. Wheeler, *Parallel multigrid and domain decomposition algorithms for elliptic equations*, in Fifth International Symposium on Domain Decomposition Methods for Partial Differential Equations, D. Keyes *et al.*, eds., SIAM, Philadelphia, 1992, pp. 376–385.

[12] P. J. Davis, *Interpolation and Approximation*, Dover Publications, New York, 1975.

[13] J. Douglas, Jr. and J. E. Roberts, *Global estimates for mixed methods for second order elliptic equations*, Math. Comp., 44 (1985), pp. 39-52.

[14] T. F. Dupont, and P. T. Keenan, *Superconvergence and postprocessing of fluxes from lowest order mixed methods on triangles and tetrahedra*, SIAM J. Sci. Stat. Comp., to appear.

[15] R. Durán, *Superconvergence for rectangular mixed finite elements*, Numer. Math., 58 (1990), pp. 287–298.

[16] R. E. Ewing, R. D. Lazarov, and J. Wang, *Superconvergence of the velocity along the Gauss lines in mixed finite element methods*, SIAM J. Numer. Anal., 28 (1991), pp. 1015–1029.

[17] L. Gastaldi and R. Nochetto, *Optimal L^∞-error estimates for nonconforming and mixed finite element methods of lowest order*, Numer. Math., 50 (1987), pp. 587-611.

[18] R. Glowinski, W. Kinton, and M. F. Wheeler, *Acceleration of domain decomposition algorithms for mixed finite elements by multi-level methods*, in Third International Symposium on Domain Decomposition Methods for Partial Differential Equations, T. F. Chan *et al.*, eds., SIAM, Philadelphia, 1990, pp. 263-289.

[19] R. Glowinski and M. F. Wheeler, *Domain decomposition and mixed finite element methods for elliptic problems*, in First International Symposium on Domain Decomposition Methods for Partial Differential Equations, R. Glowinski *et al.*, eds., SIAM, 1988, pp. 144-172.

[20] P. T. Keenan, *RUF 1.0 user manual: the Rice unstructured flow code*, Technical Report TR94–30, Department of Computational and Applied Mathematics, Rice University (1994).

[21] P. T. Keenan, *An efficient postprocessor for velocities from mixed methods on triangular elements*, Technical Report TR94–22, Department of Computational and Applied Mathematics, Rice University (1994).

[22] J. Koebbe, *A computationally efficient modification of mixed finite element methods for flow problems with full transmissivity tensors*, Numer. Meth. for PDE's, 9 (1993), pp. 339–355.

[23] H.-O. Kreiss, T. A. Manteuffel, B. K. Swartz, B. Wendroff, and A. B. White, *Supra-convergent schemes on irregular grids*, Math. Comp., 47 (1986), pp. 511–535.

[24] M. Nakata, A. Weiser, and M. F. Wheeler, *Some superconvergence results for mixed finite element methods for elliptic problems on rectangular domains*, in The Mathematics of Finite Elements and Applications V, J. R. Whiteman, ed., Academic Press, 1985.

[25] J. C. Nedelec, *Mixed finite elements in* $\mathbf{R}^3$, Numer. Math., 35 (1980), pp. 315-341.

[26] V. J. Parr, *Preconditioner schemes for elliptic saddle-point matrices based upon Jacobi multi-band polynomial matrices*, Ph.D. Thesis, Dept. of Computational and Applied Math., Rice University, 1994.

[27] D. W. Peaceman, *Fundamentals of numerical reservoir simulation*, Elsevier, 1977.

[28] R. A. Raviart and J. M. Thomas, *A mixed finite element method for 2nd order elliptic problems*, in Mathematical Aspects of the Finite Element Method, Lecture Notes in Math, 606, Springer-Verlag, New York, 1977, pp. 292-315.

[29] T. F. Russell and M. F. Wheeler, *Finite element and finite difference methods for continuous flows in porous media*, Chapter II, in The Mathematics of Reservoir Simulation, R. E. Ewing, ed., Frontiers in Applied Mathematics 1, SIAM, 1983, pp. 35–106.

[30] T. Rusten, *Iterative methods for mixed finite element systems*, Ph.D. Thesis, Dept. of Informatics, University of Oslo, 1991.

[31] J. M. Thomas, These de Doctorat d'etat, à l'Universite Pierre et Marie Curie, 1977.

[32] A. N. Tikhonov and A. A. Samarskii, *Homogeneous difference schemes on non-uniform nets*, Zh. Vychisl. Mat. i Mat. Fiz., 2 (1962), pp. 812–832, in Russian; U.S.S.R. Comput. Math. and Math. Phys., 2 (1962), pp. 927–953, in English.

[33] A. Weiser and M. F. Wheeler, *On convergence of block-centered finite-differences for elliptic problems*, SIAM J. Numer. Anal., 25 (1988), pp. 351-375.

[34] M. F. Wheeler, K. R. Roberson, and A. Chilakapati, *Three-dimensional bioremediation modeling in heterogeneous porous media*, in Computational Methods in Water Resources IX, Vol. 2: Mathematical Modeling in Water Resources, T. F. Russell *et al.*, eds., Computational Mechanics Publications, Southampton, U. K., 1992, pp. 299–315.